Tryptophan Residues at Subunit Interfaces Used as Fluorescence Probes To Investigate Homotropic and Heterotropic Regulation of Aspartate Transcarbamylase†

Luc Fetler,*,‡ Patrick Tauc,§ Guy Hervé,‡ Raymond Cunin,|| and Jean-Claude Brochon§

Laboratoire de Biochimie des Signaux Régulateurs Cellulaires et Moléculaires, UMR-CNRS 7631, Université Pierre et Marie Curie, 96 bd. Raspail, 75006 Paris, France, Laboratoire de Biotechnologies et Pharmacologie Génétique Appliquée, UMR-CNRS 8532, Ecole Normale Supérieure de Cachan, 61 av. du Président Wilson, 94235 Cachan, France, and Laboratorium voor Erfelijkheidsleer en Microbiologie, Vrije Universiteit Brussel, and Department of Microbiology, Flanders Interuniversity Institute for Biotechnology (VIB), 1 E. Grysonlaan, B-1070 Brussels, Belgium

Received December 27, 2000; Revised Manuscript Received April 10, 2001

ABSTRACT: The homotropic and heterotropic interactions in *Escherichia coli* aspartate transcarbamylase (EC 2.1.3.2) are accompanied by various structure modifications. The large quaternary structure change associated with the T to R transition, promoted by substrate binding, is accompanied by different local conformational changes. These tertiary structure modifications can be monitored by fluorescence spectroscopy, after introduction of a tryptophan fluorescence probe at the site of investigation. To relate unambiguously the fluorescence signals to structure changes in a particular region, both naturally occurring Trp residues in positions 209*c* and 284*c* of the catalytic chains were previously substituted with Phe residues. The regions of interest were the so-called 240's loop at position Tyr240*c*, which undergoes a large conformational change upon substrate binding, and the interface between the catalytic and regulatory chains in positions Asn153*r* and Phe145*r* supposed to play a role in the different regulatory processes. Each of these tryptophan residues presents a complex fluorescence decay with three to four independent lifetimes, suggesting that the holoenzyme exists in slightly different conformational states. The bisubstrate analogue *N*-phosphonacetyl-L-aspartate affects mostly the environment of tryptophans at position 240*c* and 145*r*, and the fluorescence signals were related to ligand binding and the quaternary structure transition, respectively. The binding of the nucleotide activator ATP slightly affects the distribution of the conformational substates as probed by tryptophan residues at position 240*c* and 145*r*, whereas the inhibitor CTP modifies the position of the C-terminal residues as reflected by the fluorescence properties of Trp153*r*. These results are discussed in correlation with earlier mutagenesis studies and mechanisms of the enzyme allosteric regulation.

Allosteric enzymes are characterized by the regulation of their activity by effectors which bind to the enzyme at sites different from the active sites. The description of the signaling pathways connecting these sites, as well as the relationship between local and global structure changes related to how the effectors affect the active site properties, remains a challenging problem in structural biology (*1*).

Aspartate transcarbamylase from *Escherichia coli* (ATCase,[1] EC 2.1.3.2), one of the paradigmatic allosteric enzymes (*2*, *3*), catalyzes the first step of the pyrimidine biosynthetic pathway, the carbamylation of the amino group of aspartate by carbamyl phosphate (*4*). This dodecameric 306 kDa protein consists of two catalytic trimers and three regulatory dimers, $(c_3)_2(r_2)_3$, assembled with quasi-D_3 symmetry. The isolated catalytic subunits (c_3) carrying the active sites are fully active, although devoid of regulatory properties and cooperativity for substrate binding, whereas the regulatory subunits bear the binding sites for the nucleotide effectors, but do not exhibit any catalytic activity (*5*). The holoenzyme displays homotropic cooperativity between the catalytic sites for the binding of the substrate aspartate (*6*, *7*). This phenomenon has been interpreted within the framework of the seminal concerted two-state model proposed by Monod, Wyman, and Changeux (*8*), i.e., a reversible transition between a low-affinity T-state and a high-affinity R-state. The crystal structures of these two states of ATCase, the unliganded enzyme (T-structure) and the enzyme complexed with the bisubstrate analogue *N*-(phosphonoacetyl)-L-aspartate (PALA) (R-structure) (*9*−*11*), were determined by Lipscomb and collaborators. The most prominent movements of the T to R transition are a 10.8 Å separation of the two catalytic trimers along the 3-fold axis, a 12° mutual reorientation around this same axis, and a 15°

† This work was supported by the Centre National de la Recherche, the Institut National de la Santé et de la Recherche Médicale, Université Pierre et Marie Curie, and by grants from the European Economic Community (BAP-0478-F), NATO (0364/88), the Fonds voor Wetenschappelijk Onderzoek-Flanders (G.0040.96), and the Research Council (OZR) of the Vrije Universiteit Brussel.

* To whom correspondence should be addressed. Phone: +33 1 53 63 40 80. Fax: +33 1 42 22 13 98. E-mail: fetler@ccr.jussieu.fr.

‡ Université Pierre et Marie Curie.

§ Ecole Normale Supérieure de Cachan.

|| Vrije Universiteit Brussel and Flanders Interuniversity Institute for Biotechnology.

[1] Abbreviations: ATCase, aspartate transcarbamylase; Asn (N), asparagine; c, catalytic chain; NATA, *N*-acetyl-L-tryptophanamide; PALA, *N*-(phosphonoacetyl)-L-aspartate; Phe (F), phenylalanine; r, regulatory chain; Trp (W), tryptophan; Tyr (Y), tyrosine. The letter *c* or *r* following the residue type and number indicates whether the residue belongs to the catalytic or regulatory chain.

10.1021/bi0029494 CCC: $20.00
Published on Web 07/06/2001

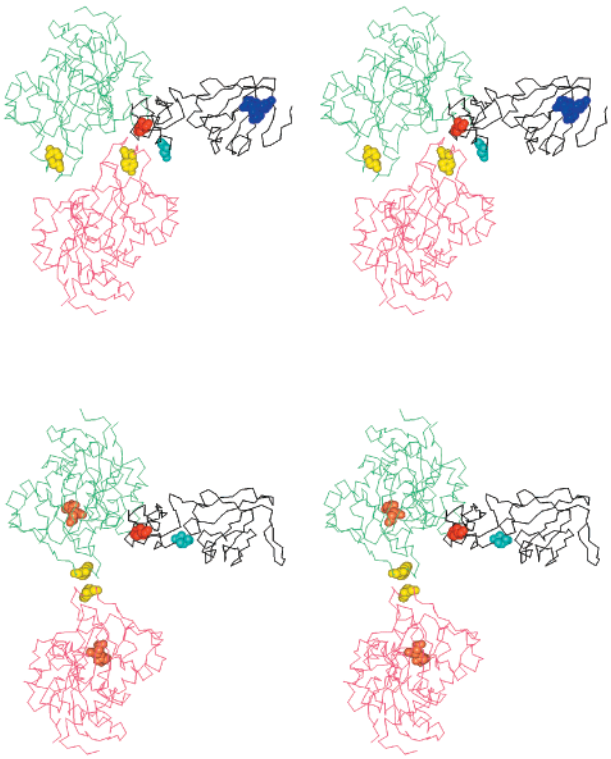

FIGURE 1: Stereoviews of the α-carbon trace of the c1 (green), c4 (magenta), and r1 chains (black) in either the T-state (top) or R-state (bottom). The other catalytic and regulatory chains were omitted for the sake of clarity. The view is oriented perpendicular to the C2 axis of the regulatory chain. CTP (dark blue) and the bisubstrate analogue PALA (orange) are represented in space-filled forms as well as residues Tyr240*c* (yellow), Phe145*r* (red), and Asn153*r* (light blue). The coordinates of ATCase were taken from the Protein Data Bank (*71*), entries 1RAI (T-state structure with CTP) (*70*) and 1D09 (R-state structure with PALA) (*62*). The graphics program WebLab ViewerLite 3.7 from Molecular Simulations Inc. was used.

rotation of the three regulatory dimers around the three 2-fold axes. These movements are even about 30% larger in solution as shown by comparing small-angle X-ray scattering data to calculated scattering profiles (*12*). This global structure change is accompanied by various tertiary structure modifications, among which is the domain closure in the catalytic chains related to the movement of the 240's loop, a region composed of residues 230*c*−245*c*. During this structure transition, the different interfaces between the catalytic and regulatory chains are remodeled. In the T-state, each regulatory chain interacts with two catalytic chains belonging to different trimers, resulting in the r1−c1 and r1−c4 types of interfaces (Figure 1). In the R-state enzyme, the r1−c4 interfaces disappear, whereas the r1−c1 type interface is only slightly modified with respect to the T-state. Numerous studies showed the allosteric nature of this enzyme whose activity is feedback-inhibited by CTP and UTP, the end products of the pyrimidine pathway, and stimulated by the purine nucleotide ATP (*6*, *13*). This heterotropic regulation was first interpreted within the framework of the Monod−Wyman−Changeux model (*14*, *15*), ATP promoting the T to R transition and CTP favoring the reverse. The experimental uncoupling of the homotropic and heterotropic effects led to the proposal of other mechanisms [reviewed by Hervé (*2*) and Lipscomb (*3*)]. According to these models, the nucleotide effectors promote local conformational changes that are transmitted either to the catalytic sites (*16*−*18*) or only to the interfaces between regulatory and catalytic subunits (*19*). Their actions can also be viewed as indirect effects transmitted through the interface of the regulatory chains (*20*).

To obtain a physical signature of the local conformational changes related to the regulatory mechanisms of ATCase, we used tryptophan fluorescence spectroscopy, a valuable technique for exploring the events associated with ligand binding. The tryptophan probe, which is very sensitive to a wide variety of environmental conditions (*21*), yields structural and dynamic information about its surroundings. The technique is especially relevant when mutant proteins with a single tryptophan residue at the site of interest are available. To meet this requirement, the natural ATCase tryptophan residues at positions 209*c* and 284*c* were replaced with nonfluorescent phenylalanines (*22*) before introducing a tryptophan probe in the region being investigated. Thus, Trp residues inserted at either position 153*r* or 145*r* in the C-terminal part of the regulatory chain (Figure 1) enabled exploration of the r1−c4 interface, which is supposed to be involved in the cooperative and allosteric regulations (*19*, *23*−*25*), especially in activation by ATP (*26*). The 240's loop, structurally related to the c1−c4 and r1−c4 interfaces, supposed to play a crucial role in the formation of the high-affinity active sites and the quaternary structure transition (*27*), was probed through a tryptophan introduced at position 240*c*.

This work addresses two main questions concerning the interfaces. Can the fluorescence signals be related to the T to R structure transition, or are they only sensitive upon substrate binding as shown for the 240's loop in a previous work (*22*)? Is it possible to gain some information about the intramolecular signaling used to activate or inhibit the enzyme activity upon effector binding to the regulatory chain? Both questions were addressed by analyzing the fluorescence properties of single-tryptophan mutants by steady-state and time-resolved fluorescence measurements.

EXPERIMENTAL PROCEDURES

Chemicals. Carbamyl phosphate (lithium salt), L-aspartate, adenosine triphosphate (sodium salt), and cytidine triphosphate (sodium salt) were purchased from Sigma Chemical Co. Tris(hydroxymethyl)aminomethane (Tris) was from Merck, and L-[U-^{14}C]aspartate (300 mCi/mmol) was from CEA-Saclay. PALA was a generous gift from V. Narayanan and L. Kedda of the Drug Synthesis and Chemistry Branch, Division of Cancer Treatment, National Institutes of Health, Silver Spring, MD. Restriction enzymes were from New England Biolabs. T4 polynucleotide kinase, T4 ligase, and the Klenow fragment of DNA polymerase I were from Pharmacia. The plasmid pUC 119 and the phage M13K07 were obtained from J. Messing (Rutgers University, Camden, NJ).

Construction of Mutant ATCases, Enzyme Preparation, and Assay. In the three mutant enzymes studied here, the two naturally occurring tryptophans at positions 209 and 284 of the catalytic chain had been substituted with phenylalanines (W209F/W284F). Tyr240*c*, Phe145*r*, and Asn153*r* were then replaced with tryptophans to obtain the W209F/W284F/Y240*c*W, W209F/W284F/F145*r*W, and W209F/W284F/N153*r*W enzymes, respectively. W209F/W284F/

Y240*c*W was prepared by site-directed mutagenesis as previously described (*22*). The kinetic and regulatory properties of the mutants in the regulatory chain had been studied before in an otherwise wild-type ATCase context (*26*, *28*). The mutations were imported in the plasmid carrying the W209F/W284F ATCase genes on 630 bp *Hpa*I−*Sal*I DNA cassettes which had been verified by sequencing.

The wild-type and modified forms of the enzyme were purified as previously described (*22*). The ATCase activity was measured in 50 mM Tris-HCl buffer at pH 8.0, in the presence of saturating (5 mM) carbamyl phosphate using a radioactive assay (*29*). The stimulation of the enzyme activity by the bisubstrate analogue PALA was tested in the presence of 5 mM carbamyl phosphate and $^1/_{10}$ of the respective $[S]_{0.5}$ values in the presence of increasing concentrations of PALA. The relative activity in the presence of PALA is expressed as compared to the reaction in the absence of this compound. The percentage of stimulation or inhibition of ATCase activity by the nucleotides is defined as the ratio of the difference in activity of the enzyme in the presence and absence of the effector, to the activity in the absence of the effector.

Steady-State Fluorescence. Fluorescence emission spectra were recorded at 20.0 ± 0.1 °C in 50 mM Tris-HCl buffer (pH 7.0) on an SLM 8000 spectrofluorometer in the L-format configuration. The fluorescence spectra were recorded with both polarizers set in the vertical position. The excitation and emission bandwidths were set at 4 and 2 nm, respectively. The excitation wavelength was 300 nm. The fluorescence spectra were collected through an additional 1 M $CuSO_4$ filter (1 cm optical path). The rhodamine reference signal was used to correct fluctuations of the excitation light. Each fluorescence spectrum $F(\lambda)$ was corrected for the Raman scattering light and the background signal by subtracting a corresponding buffer spectrum $R(\lambda)$. To correct any spectral shift, the spectra were normalized against NATA spectra $N(\lambda)$. Since the emission bandwidth is sufficiently small, the center of gravity (in nanometers) of the emission spectra $F(\lambda)$ can be approximated by (*30*)

$$\mathrm{CG} = \frac{\sum_{i=n}^{m} \lambda_i^{-2} F(\lambda_i)}{\sum_{i=n}^{m} \lambda_i^{-3} F(\lambda_i)} \quad (1)$$

with the wavelength λ_i sampled over the entire emission spectrum in 0.5 nm intervals. The fluorescence emission spectra of the different enzymes in the presence of PALA, CTP, or ATP were directly corrected for dilution and inner filter effects. This correction factor was calculated from measurements of the fluorescence emission of a NATA solution containing the same concentration of substrate analogue or effector. To compare the CG of the enzymes measured in different experiments, their position was calibrated against NATA. This explains the 8 nm shift for the W209F/W284F/Y240*c*W mutant as compared to a previously published result (*22*). The bisubstrate analogue PALA was used to titrate the active sites. Since the concentration of active sites used in these experiments was ~2000-fold higher than the dissociation constant of PALA for the wild-type enzyme (K_D = 30 nM) (*31*, *32*), assumed to be close to that of the mutant enzymes on the basis of the comparison of the $[S]_{0.5}$ for aspartate, virtually no PALA was left free in solution. Thus, the fractional saturation function $\bar{Y}$ can be directly related to the concentration of PALA added.

Time-Resolved Fluorescence Measurements. Fluorescence decay was assessed by the single-photoelectron counting method (*33*). All experiments were carried out using a picosecond laser system as an excitation source. The apparatus consisted of a mode-locked, cavity-dumped dye laser system (rhodamine 6G), synchronously pumped by an Ar^+ laser, providing 10−15 ps pulses at 0.8 MHz. Using a double-harmonic generator, the samples were excited at 300 nm, and emitted photons were detected at 350 nm, with a Jobin-Yvon H10 monochromator with a bandwidth of 16 nm, by a microchannel plate photomultiplier (Hamamatsu R1564U). The instrumental response was 80−100 ps (full width at half-maximum). Further details of the laser spectrometer have been published elsewhere (*34*), as the optical and electronic parts of the instrumental setup (*35*). The fluorescence of 1 mL samples was measured in a 5 mm × 10 mm quartz cuvette. Data for $I_{vv}(t)$ and $I_{vh}(t)$ were stored in separate memories of a plug-in multichannel analyzer card (Canberra) in a Deskpro 286E microcomputer. Time sampling was 25 ps per channel, and 2048 channels were used to store the decays. The correction factor G for the polarization bias was determined from the depolarized fluorescence of NATA at 20 °C under identical optical conditions (*36*). Routinely, 5×10^6 to 5×10^7 counts were stored for the $I_{vv}(t)$ fluorescence intensity decay. The instrumental response function was determined by measuring the light scattered by a Ludox solution close to the emission wavelength.

Data Analysis. Data analysis of the total fluorescence intensity $I(t)$ and fluorescence anisotropy $A(t)$ was performed by the quantified maximum entropy method (MEM) (*37*−*39*) using FAME5 and FAME-QT programs (MEDC Ltd.). After excitation by a vertically polarized pulse of light, the fluorescence intensity at time t after the start of the excitation is

$$I(t) = I_{vv}(t) + 2GI_{vh}(t) = E_\lambda(t) \otimes \int_0^\infty \alpha(\tau) e^{(-t/\tau)}\, d\tau \quad (2)$$

where $I_{vv}(t)$ and $I_{vh}(t)$ are the two polarized components of the fluorescence intensity at time t, $E_\lambda(t)$ is the temporal shape of the instrumental function, ⊗ denotes a convolution product, and $\alpha(\tau)$ is the lifetime distribution, i.e., the number of fluorophores with lifetime τ.

A lifetime domain spanning 150 values equally spaced on a logarithmic scale between 0.01 and 15 ns was routinely used. A channel of a null lifetime corresponding to the scattered light was added. Up to 200 iterations were run for these analyses. The center $\langle\tau_j\rangle$ of a single class j of lifetimes over the $\alpha_i(\tau_i)$ distribution is defined as

$$\langle\tau_j\rangle = \frac{\sum_{i_1}^{i_2} \alpha_i(\tau_i)\tau_i}{\sum_{i_1}^{i_2} \alpha_i(\tau_i)} \quad (3)$$

the summation being performed on the significant values of

Table 1: Kinetic Parameters of the Wild-Type and Modified Forms of ATCase[a]

	V_m	$[S]_{0.5}$ (mM)	n_H	PALA (ra)	ATP (%)	CTP (%)
wild type	24.2 ± 0.5	16.3 ± 0.5	2.8 ± 0.2	3.9	240	65
W209F/W284F	28.3 ± 1.1[b]	25.7 ± 1.2[b]	2.6 ± 0.2[b]	3.7[b]	160	60
W209F/W284F/Y240*c*W	15.7 ± 0.5[b]	52.1 ± 2.4[b]	2.3 ± 0.2[b]	3.4[b]	155	60
W209F/W284F/N153*r*W	28.9 ± 1.0	20.6 ± 0.9	2.4 ± 0.2	3.9	135	60
W209F/W284F/F145*r*W	32.5 ± 2.2	10.6 ± 0.9	2.1 ± 0.2	1.9	135	60

[a] These parameters were calculated as described in Experimental Procedures through a computer fit by a nonlinear least-squares procedure to either the Hill equation or the Michaelis−Menten equation. V_m is the maximal velocity expressed in millimoles per hour per milligram of protein. n_H is the Hill coefficient. PALA stimulation is expressed as relative activity (ra). The values correspond to the highest level of stimulation observed when the reaction velocity in the absence of PALA is made 1. [b] Taken from previous work (*22*).

$\alpha_i(\tau_i)$ for the j class. C_j is the normalized contribution of the lifetime class j:

$$C_j = \frac{\sum_{i_1}^{i_2} \alpha_i(\tau_i)}{\sum_{i=1}^{i=150} \alpha_i(\tau_i)} \quad (4)$$

RESULTS

Rationale for the Construction of the Modified ATCases. The steady-state kinetic properties of the tryptophan-free mutant W209F/W284F, in which both naturally occurring Trp residues at positions 209*c* and 284*c* are replaced with Phe residues, are nearly identical to those of the wild-type enzyme, except for a slight decrease in the affinity for the substrate aspartate and ATP activation (Table 1). Substituting a defined residue within this neutral mutant protein with a fluorescent Trp allowed us to trace eventual static or dynamic conformational changes in the close vicinity of the probe, related to substrate or nucleotide binding. In this study, we focused on the interface between the 240's loop of the catalytic chain and the C-terminal region of the regulatory chain. This interface is ruptured during the cooperative transition (Figure 1) and appears to be involved in the allosteric regulation of the enzyme by nucleotides. Therefore, the modifications in the fluorescence properties upon substrate analogue or nucleotide effector binding were studied in the three mutant proteins W209F/W284F/Y240*c*W, W209F/W284F/F145*r*W, and W209F/W284F/N153*r*W.

Kinetic Properties of the Mutant ATCases. The kinetic parameters as deduced from the saturation curves of the mutant enzymes are presented in Table 1. Replacing Tyr240*c* with a Trp in the W209F/W284F background causes a decrease in both the maximal velocity and the affinity for aspartate, the homotropic interactions being conserved. W209F/W284F/N153*r*W and W209F/W284F/F145*r*W mutants have steady-state kinetic properties which are very similar to those of wild-type ATCase despite a slight decrease in the Hill coefficient for the latter one, accompanied by an increase in its affinity for aspartate. In the presence of a low concentration of aspartate, the bisubstrate analogue PALA increases the rate of the reaction by promoting the T to R transition (*31*). The extent of this stimulation of the activity of the mutant enzymes by PALA is presented in Figure 2. The mutants containing a Trp residue in either position 145*r* or 153*r* exhibit an enhanced activity in the presence of this compound, though to a lesser extent for the W209F/W284F/F145*r*W ATCase. W209F/W284F/Y240*c*W requires a 3-fold higher concentration of PALA than the wild-type ATCase to reach a similar stimulation, a result which is consistent with the higher $[S]_{0.5}$ value for aspartate of this mutant. Taken together, these kinetic data indicate that all three modified enzymes are able to undergo the T to R transition.

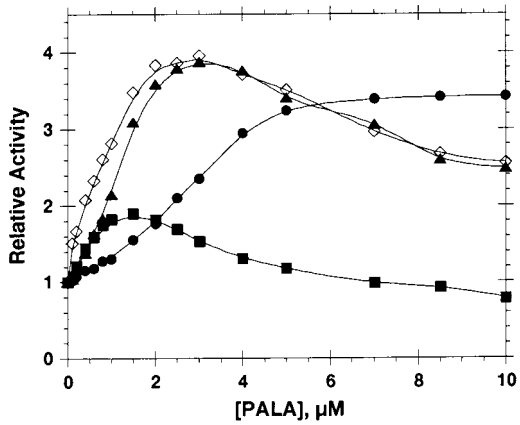

FIGURE 2: Stimulation of the ATCase reaction by PALA. The reaction was performed as indicated in Experimental Procedures: (◇) wild-type ATCase, (●) W209F/W284F/Y240*c*W, (▲) W209F/W284F/N153*r*W, and (■) W209F/W284F/F145*r*W.

The influence of ATP and CTP on the rate of the reaction catalyzed by the mutants is presented in Figure 3. All three mutant enzymes studied here have a similarly decreased sensitivity to ATP, suggesting that the residues at these positions are involved in the mechanism of ATP regulation either directly or indirectly (*26*, *40*, *41*). The three mutant enzymes show no alteration of their response to the allosteric inhibitor CTP. The comparison of the kinetic results presented here to those obtained with mutant ATCases harboring the same substitutions at position 240*c*, 153*r*, or 145*r*, but in an otherwise wild-type context (*26*), confirms that replacing both naturally occurring Trp residues at positions 209*c* and 284*c* with Phe residues does not significantly perturb the enzyme kinetic and regulatory properties.

Steady-State Fluorescence. The steady-state fluorescence emission spectra of the three modified forms of ATCase differ as shown by their respective center of gravity (Figure 4A). The corresponding values are <355 nm which is the standard of the NATA tryptophanyl moiety in a buffer solution (*42*). The center of gravity of the W209F/W284F/F145*r*W mutant is blue shifted by about 4 nm as compared to those of the other two mutant enzymes, in accordance with the more buried position of this residue in the r1−c4 interface (Figure 1). The fluorescence emission spectrum of the W209F/W284F/Y240*c*W ATCase is red shifted by 4 nm upon PALA binding, this change being directly proportional

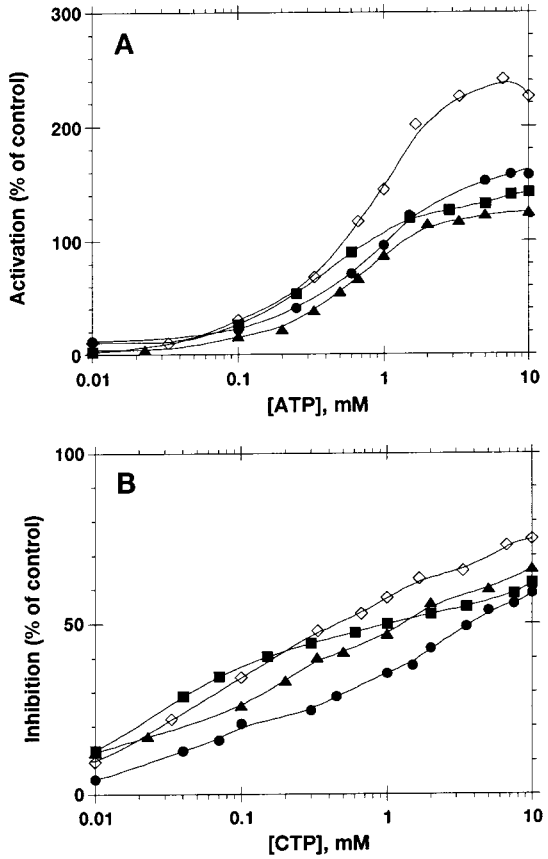

FIGURE 3: Influence of the nucleotide effectors on the activity of ATCase and its modified forms. The influences of ATP (A) and CTP (B) on the rate of reaction were determined, and the percentages of stimulation were calculated as described in Experimental Procedures: (◇) wild-type ATCase, (●) W209F/W284F/Y240*c*W, (▲) W209F/W284F/N153*r*W, and (■) W209F/W284F/F145*r*W.

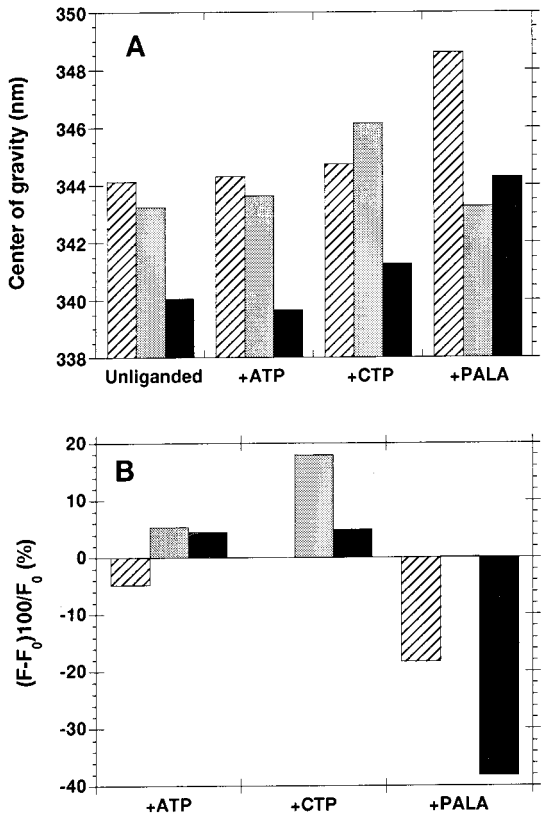

FIGURE 4: Position of the center of gravity (A) and relative intensity (B) of the fluorescence emission spectra of the mutant ATCases. The relative fluorescence is based upon integration of emission spectra in the presence (F) and absence (F_0) of either ATP (5 mM), CTP (5 mM), or PALA (3.3×10^{-4} M) as described in Experimental Procedures: hatched bars, W209F/W284F/Y240*c*W; gray bars, W209F/W284F/N153*r*W; and black bars, W209F/W284F/F145*r*W.

to the extent of saturation of the active sites (*22*), whereas the fluorescence intensity decreases by ~20% (Figure 4). Saturating amounts of CTP do not significantly modify the fluorescence properties of this mutant, whereas ATP reduces the relative fluorescence intensity by only 5%, close to the limit of the accuracy of the present measurements. The fluorescence spectrum of the W209F/W284F/N153*r*W ATCase is not modified upon PALA binding. CTP induces a red shift of ~2 nm and increases the relative fluorescence intensity by 18% as compared to that of the unliganded enzyme (Figure 4). The modifications induced by ATP are minor. The fluorescence spectrum of the W209F/W284F/F145*r*W ATCase is peculiarly sensitive to the binding of the bisubstrate analogue as shown by a 4 nm increase in the center of gravity, indicative of an enhanced exposure of the Trp residue to solvent, and a nearly 40% decrease in the total fluorescence intensity (Figure 4). Both nucleotides increase the fluorescence intensity by 5%, but only CTP induces a 1 nm red shift of the center of gravity.

Titration of the Structure Transition of W209F/W284F/F145rW ATCase with PALA. The 4 nm red shift signal upon PALA binding and the major decrease in the fluorescence intensity of this enzyme have been used in titration experiments with this bisubstrate analogue. Since virtually all the PALA added in a substoichiometric amount is bound to the enzyme, the saturation function $\bar{Y}$ can be directly related to the concentration of PALA added (see Experimental Procedures). As shown in Figure 5, the titration of W209F/W284F/F145*r*W with PALA indicates that the change in the level of exposure of the Trp residue to solvent precedes the saturation function $\bar{Y}$ and reaches its maximum when an average of four active sites out of six are occupied. Such a variation is expected for a cooperative enzyme if the probe reports on the $\bar{R}$-state function, which is the fraction of molecules in the R quaternary structure, and is indeed observed when monitoring the quaternary structure change by small-angle X-ray scattering (*22*, *43*).

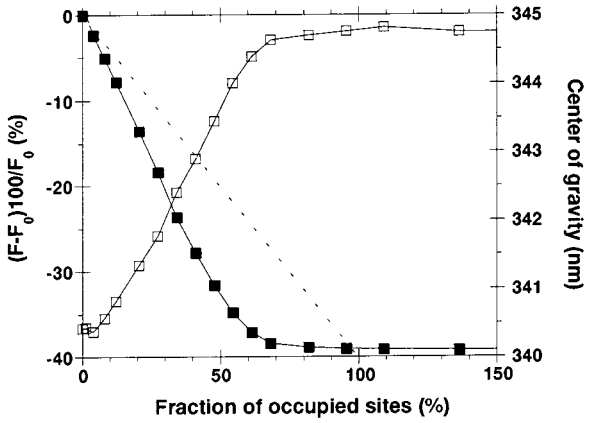

FIGURE 5: PALA titration curves of W209F/W284F/F145*r*W ATCase (□, center of gravity; ■, relative fluorescence intensity). The experimental conditions are described in Experimental Procedures. The dashed line corresponds to the saturation function $\bar{Y}$.

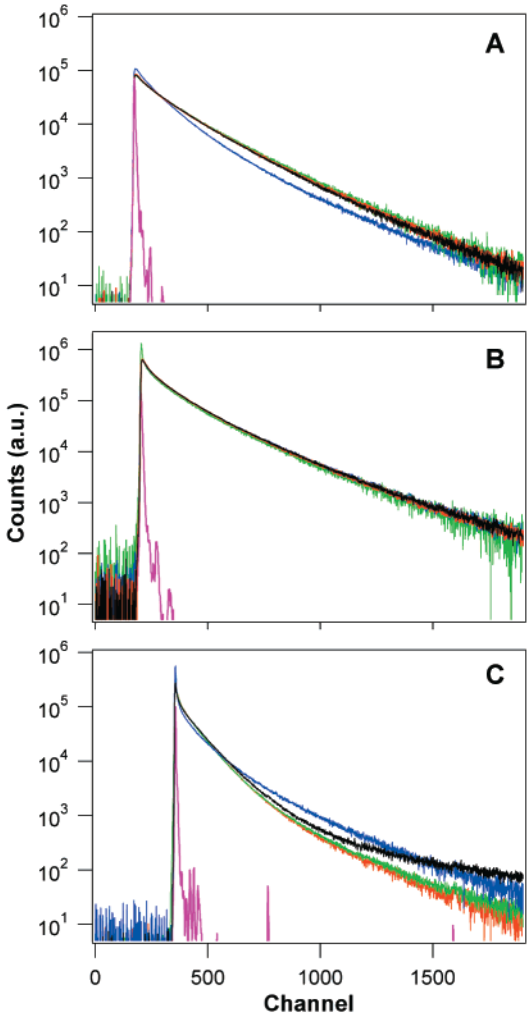

FIGURE 6: Normalized total fluorescence intensity decays of ATCase and its modified forms [(A) W209F/W284F/Y240*c*W, (B) W209F/W284F/N153*r*W, and (C) W209F/W284F/F145*r*W] either unliganded (black) or in the presence of 5 mM ATP (red), 5 mM CTP (green), or 3.3×10^{-4} M PALA (blue). The flash (magenta) is the instrumental response function. One channel equals 25 ps. The experimental conditions are described in Experimental Procedures.

Time-Resolved Fluorescence. Time-resolved fluorescence is particularly sensitive to the details of the local environment of a fluorescent chromophore and can provide information about local structure microheterogeneity which is not accessible by steady-state fluorescence.

(a) W209F/W284F/Y240cW ATCase. The normalized fluorescence intensity decays of the W209F/W284F/Y240*c*W ATCase are presented in Figure 6A, and the corresponding pre-exponential coefficients are reported in Table 2A for the various experimental conditions. Fluorescence lifetime distributions obtained with the W209F/W284F/Y240*c*W enzyme display three main components centered at 0.67 (18%), 2.6 (34%), and 5.3 ns (48%), respectively. Occasionally, a longer lifetime of ~8 ns, having a relative contribution of less than 5%, could be found. Since the associated error bars to the surface and the centroid of this peak are very large, this minor component is regarded as artifactual and no longer presented in the results below. At saturating concentrations, PALA decreases the longest lifetime τ_3 by 1.1 ns, and the relative proportion of the two lifetimes, τ_2 and τ_3, are almost inverted as compared to those of the unliganded enzyme (Table 2A). As a direct consequence, the mean lifetime decreases by 29%. The same kind of analysis was performed on the catalytic subunits of W209F/W284F/Y240*c*W. A lifetime distribution similar to that of the holoenzyme is observed, comprising three principal peaks around 0.67 (17%), 2.4 (24%), and 4.7 ns (59%). When PALA binds, only the proportions of both longer lifetimes, τ_2 and τ_3, change in the same proportion as for the holoenzyme, resulting in a decrease in the mean lifetime of 14%. Binding of saturating amounts of either nucleotide, ATP or CTP, to the holoenzyme has no major effect on the fluorescence intensity decays (Figure 6A). Data analysis shows that the fluorescence mean lifetime is decreased by 7% in the presence of ATP and that τ_3 is slightly increased in the presence of CTP as compared to the unliganded enzyme (Table 2A). These parameter changes may result from subtle local structure changes upon ATP or CTP binding.

(b) W209F/W284F/N153rW ATCase. The fluorescence decay curves of W209F/W284F/N153*r*W enzyme are described by four lifetimes, centered at 0.3 (14%), 0.7 (25%), 2.8 (35%), and 6.2 ns (25%) (Figure 6B and Table 2B). A very short lifetime between 20 and 55 ps, at the limit of the resolution of our experimental setup, has been found under the different experimental conditions. However, as its relative contribution to the fluorescence intensity does not exceed 1%, we did not further consider this very short lifetime. Addition of saturating amounts of either PALA or ATP did not change the fluorescence decay (Figure 6B) or the lifetime distribution parameters (Table 2B). The binding of CTP results in a 9% decrease of the mean lifetime due essentially to a slight shortening of τ_3 and τ_4. The discrepancy between these minor changes and the pronounced modifications of the steady-state fluorescence emission spectrum in the presence of CTP can be explained by the disappearance of a static quenching from a neighboring residue.

(c) W209F/W284F/F145rW ATCase. The fluorescence decay curves (Figure 6C) of W209F/W284F/F145*r*W ATCase are represented by four different lifetimes, centered around 0.13 (37%), 0.4 (22%), 2.1 (27%), and 3.5 ns (14%) (Table 2C). A shorter lifetime around 20 ps was observed as for the former mutant and considered artifactual. The marked reduction in the lifetime values of this enzyme as compared to both previous mutants, although Trp145*r* is relatively protected from the solvent (Figures 1 and 4), arises from dynamic quenching of neighbor residues. In the presence of the bisubstrate analogue PALA, all fluorescence lifetimes are shortened and their respective contributions are modified, resulting in a 42% decrease in the mean lifetime (Table 2C). Both nucleotides significantly modify the lifetime distribution of the enzyme, in a manner similar though not identical to the binding of PALA. The major difference between the nucleotide effectors ATP and CTP with regard to the fluorescence decay curves concerns the disappearance of the shorter lifetime τ_1 in the presence of ATP. Thus, the environment changes in the vicinity of residue 145*r* are distinctly related to the various ligands that are tested.

Anisotropy Decays. The fluorescence anisotropy decays were measured under the same conditions described above, in the presence and absence of ligands. A single rotational correlation time without any evidence for internal flexibilities in the nanosecond domain was found for the three enzymes studied here. In addition, the r_0 values of initial anisotropy

Table 2: Effects of Ligand Binding on the Fluorescence Intensity Decay Parameters of the Mutant W209F/W284F/Y240*c*W, W209F/W284F/N153*r*W, and W209F/W284F/F145*r*W[a]

(A) Mutant W209F/W284F/Y240*c*W

Trp240*c*	τ_1 (ns) (c_1)	τ_2 (ns) (c_2)	τ_3 (ns) (c_3)	χ^2	$\langle\tau\rangle$ (ns)
unliganded	0.67 ± 0.05 (18 ± 1%)	2.6 ± 0.3 (34 ± 10%)	5.3 ± 0.4 (49 ± 10%)	1.08	3.60
with PALA	0.65 ± 0.03 (18 ± 1%)	2.3 ± 0.3 (52 ± 16%)	4.2 ± 0.8 (30 ± 15%)	1.09	2.57
with ATP	0.67 ± 0.04 (20 ± 1%)	2.4 ± 0.2 (31 ± 7%)	5.0 ± 0.5 (49 ± 12%)	1.16	3.33
with CTP	0.69 ± 0.08 (19 ± 2%)	2.8 ± 0.4 (39 ± 12%)	5.9 ± 0.5 (42 ± 12%)	1.07	3.70

(B) W209F/W284F/N153*r*W

Trp153*r*	τ_1 (ns) (c_1)	τ_2 (ns) (c_2)	τ_3 (ns) (c_3)	τ_4 (ns) (c_4)	χ^2	$\langle\tau\rangle$ (ns)
unliganded	0.32 ± 0.10 (14 ± 5%)	0.7 ± 0.1 (25 ± 5%)	2.8 ± 0.1 (36 ± 3%)	6.2 ± 0.3 (25 ± 2%)	0.99	2.78
with PALA	0.20 ± 0.09 (16 ± 6%)	0.7 ± 0.1 (25 ± 5%)	2.8 ± 0.4 (35 ± 6%)	6.2 ± 0.6 (24 ± 6%)	0.99	2.68
with ATP	0.28 ± 0.18 (11 ± 9%)	0.7 ± 0.2 (28 ± 9%)	2.8 ± 0.4 (37 ± 8%)	6.2 ± 0.6 (24 ± 6%)	1.05	2.75
with CTP	0.22 ± 0.22 (17 ± 8%)	0.7 ± 0.3 (26 ± 10%)	2.5 ± 0.3 (31 ± 8%)	5.9 ± 0.3 (26 ± 6%)	1.08	2.53

(C) W209F/W284F/F145*r*W

Trp145*r*	τ_1 (ns) (c_1)	τ_2 (ns) (c_2)	τ_3 (ns) (c_3)	τ_4 (ns) (c_4)	χ^2	$\langle\tau\rangle$ (ns)
unliganded	0.13 ± 0.02 (37 ± 4%)	0.40 ± 0.04 (22 ± 2%)	2.1 ± 0.1 (27 ± 3%)	3.5 ± 0.2 (14 ± 2%)	1.09	1.19
with PALA	0.08 ± 0.05 (31 ± 4%)	0.20 ± 0.04 (35 ± 3%)	0.77 ± 0.07 (15 ± 5%)	2.5 ± 0.1 (19 ± 1%)	1.06	0.69
with ATP		0.21 ± 0.01 (48 ± 4%)	0.78 ± 0.10 (14 ± 1%)	2.3 ± 0.1 (38 ± 2%)	1.10	1.08
with CTP	0.06 ± 0.02 (23 ± 11%)	0.25 ± 0.01 (37 ± 6%)	0.97 ± 0.09 (10 ± 2%)	2.3 ± 0.1 (30 ± 5%)	1.05	0.89

[a] τ_j values are the barycenters of the lifetime class j, and c_j values are the normalized areas over each class. $\langle\tau\rangle$ is the mean lifetime.

at time zero were close to 0.3, as expected for immobilized tryptophans excited at 300 nm (*44*).

DISCUSSION

Most insights into the cooperative T to R structure transition and the heterotropic regulation of ATCase were obtained by steady-state kinetics of the wild-type and numerous mutant enzymes, X-ray crystallography, and complementary methods sensitive to quaternary structure changes. In contrast to hemoglobin with its four hemes, for instance, no single intrinsic reporter groups exist in ATCase and, therefore, relatively few studies were based on techniques sensitive to local conformational changes (*45*−*48*). Here we used steady-state and time-resolved fluorescence spectroscopy of single-tryptophan ATCase mutants to investigate microenvironment changes related to the cooperative and allosteric regulation of the enzyme. The fluorescence lifetimes of tryptophan residues in proteins are very sensitive to the proximity of quenchers, especially peptide bonds and different amino acid side chains (*49*, *50*). The fluorescence decay of this residue is often multiexponential (*51*) and is generally interpreted in terms of a protein conformational heterogeneity (*52*) due to either the existence of conformational substates (*53*, *54*) or the presence of discrete species undergoing a slow exchange (*53*). In the particular case of ATCase, an additional degree of complexity in the time-resolved fluorescence signals can arise from the dodecameric and slight asymmetric nature (*3*) of this enzyme. Indeed, each particular mutant actually contains six tryptophans which might exist in slightly different environments.

Cooperative Transition. The three mutant enzymes investigated here contain a single Trp residue per r−c unit, at either position 240*c*, 145*r*, or 153*r*, and remain cooperative as shown by the respective Hill coefficient values. Furthermore, the bisubstrate analogue PALA, known to promote the T to R transition, activates the three enzymes. Thus, on the basis of steady-state kinetic measurements, the three mutants are able to undergo the T to R transition. This has already been established for the W209F/W284F/Y240*c*W enzyme using small-angle X-ray scattering (*22*). Due to cooperativity, this quaternary structure transition is complete when only an average of four of six active sites are occupied by PALA, as observed for the wild-type enzyme (*43*).

The movement of the 240's loop has been assumed to play a critical role in the formation of a high-affinity active site and thus in the quaternary structure transition and the domain closure of the remaining free catalytic sites (*55*). This statement has been questioned by monitoring the local changes in the 240's loop upon PALA binding. Indeed, the fluorescence signals of the W209F/W284F/Y240*c*W mutant holoenzyme, as well as its related catalytic subunits devoid of any cooperativity, are in direct proportion to the active site saturation and not to the cooperative T to R structure transition (*22*). A simulation of this transition predicted that the closure of the two catalytic domains occurs when the quaternary structure changes are almost complete (*56*). The absence of a strict linkage between the quaternary structure transition and the movement of the 240's loop was subsequently confirmed by the crystal structures of the isolated catalytic subunits, obtained either in the absence or in the presence of PALA (*57*, *58*). The 240's loops in the unliganded catalytic subunits, which exhibit high-affinity active sites, adopt a conformation similar to the T-state structure of the holoenzyme, while they adopt an R-like conformation in the presence of PALA. A corollary of these results should be the existence of a state of the holoenzyme, albeit scarcely populated in the case of the wild-type enzyme, in which the catalytic chains would present an open T-like conformation within an R-state quaternary structure. Some mutants in which the c1−c4 interface has been destabilized could well adopt a structure of this kind.

The properties of the tryptophan probe at position 145*r* are of potential interest for the study of the T to R transition. Indeed, its fluorescence properties are extensively modified upon PALA binding as shown by the steady-state and time-resolved fluorescence measurements. The increased level of exposure of the tryptophan to the solvent as revealed by the red shift of the fluorescence spectrum results from the

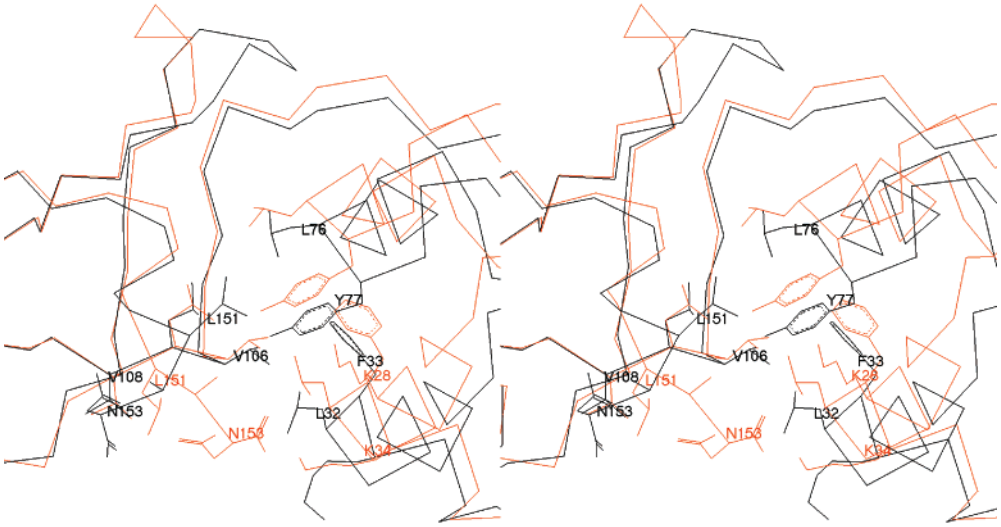

FIGURE 7: Closeup stereoview of the allosteric−zinc interface in the regulatory chain after superposition of the zinc domains from the T-state structure in the presence of CTP [PDB entry 1RAI (black)] and the R-state structure in the presence of PALA [PDB entry 1D09 (red)]. The orientation of the molecule is similar to that used in Figure 1.

disappearance of the r1−c4 interface in the R-state structure (Figure 1). The concomitant decrease in the fluorescence intensity and in the mean lifetime might result from an increased level of quenching of the tryptophan by its intrachain peptide bond and the surrounding water (*49*, *59*). However, we cannot attribute a particular lifetime to either the T- or R-state conformation. Most interestingly, the titration in the presence of PALA shows that this change in exposure to solvent of Trp145*r* reaches its maximum when only an average of four out of six active sites are occupied. Thus, the modifications of the fluorescence signal of the W209F/W284F/F145*r*W mutant upon PALA binding are related to the *R*-state function. The tryptophan in position 145*r* constitutes therefore an ideal probe for investigating the kinetics of the cooperative structure transition (*60*, *61*), or the temperature and pressure effects on the conformational equilibrium using fluorescence spectroscopy.

Steady-state and time-resolved fluorescence properties of the W209F/W284F/N153*r*W ATCase are not significantly affected by PALA binding, indicating that no major structure modification occurs in this region during the T to R structure transition, a result that was not expected on the basis of a recently refined R-state structure (*62*). This 2.1 Å resolution structure obtained in the presence of PALA (PDB entry 1D09) firmly establishes the backbone trace of the C-terminal part of the regulatory chains (Figure 7). As far as the last three regulatory chain residues are concerned, it departs from the previously determined X-ray structures, either T or R (*63*), which suffered from weak electron density maps in this region. In the new structure (1D09), the 150*r*−153*r* region is more extended, enabling the formation of an ionic bond with the side chain of Lys34*r* instead of the formerly described bond with Lys28*r* and reinforcing the hydrophobic interactions between Val150*r*, Leu151*r*, and Ala152*r* and residues Val108*r*, Leu107*r*, and Val106*r*, which are part of the hydrophobic interface separating the allosteric and zinc domain of the regulatory chain (Figure 7). Such a change in position of more than 10 Å for the C-terminal carboxyl between this R-state structure (1D09) and the unliganded T-state structure (6AT1) should have a measurable effect on the fluorescence properties of Trp153*r*, contrary to our experimental results. Therefore, we propose that the last three residues of the regulatory chain adopt in the unliganded enzyme a position similar to that described in the recent R-state structure (*62*). Only an improved crystal T-state structure will give a definite answer to that issue. We cannot formally exclude a bias in our data due to the more hydrophobic nature of the Trp residue, as compared to Asn153*r*, which could stabilize interactions with the hydrophobic residues in the allosteric−zinc interface independent of the T to R transition. However, this explanation is not consistent with the results obtained in the presence of CTP (see the next section). It is interesting to note that mutants in which Val106*r* and Leu151*r* had been substituted with bulkier residues, Trp and Gln, respectively, exhibit reduced cooperativity and an enhanced affinity for aspartate as if the T-state is destabilized (*3*). Mutagenesis studies further established that the deletion of the last two residues of the r chain abolishes cooperativity (*25*, *26*), a situation similar to that encountered with the pAR5 mutant in which the last eight residues of the regulatory chain had been replaced with a new sequence of six residues (*64*). Small-angle X-ray scattering studies demonstrated that in the absence of substrates the quaternary structure of this latter mutant is between T and R and that carbamyl phosphate alone causes a shift toward the R-state (*65*). The substitution of Asn153*r* with a glycine or with a tryptophan does not affect the kinetic parameters of the enzyme, and its deletion only reduces cooperativity (*26*). The firm conclusion of all those studies is that the presence of the last two residues is necessary to stabilize the T-state, regardless of their nature, probably through some indirect interaction with the adjacent r1−c4 interface.

Influence of the Allosteric Effectors. In the work presented here, we did not investigate the possible influence of the nucleotides on the T to R equilibrium (*43*, *66*), but rather tried to obtain a physical signature of the structural perturbations induced by both nucleotide effectors, especially at the interfaces between regulatory and catalytic chains in the T-state. X-ray crystallography showed that ATP, in the absence of substrates, increases the separation of the catalytic trimers by 0.4 Å and weakens the r1−c4 interface, whereas

CTP has no measurable effect on the separation of the trimers or on the r1−c4 interface (*67*). The global conformational changes are consistent with the view that ATP and CTP act on the conformation of the regulatory dimer, which then controls the separation twist of the catalytic trimers (*20*). The nucleotide effects must transit through the interface between the allosteric and zinc domains of the regulatory chain to reach the interface with the catalytic subunits.

(a) ATP Activation. The environment of Trp153*r* does not seem to be modified upon ATP binding as far as can be concluded from the fluorescence data. However, binding of ATP results in subtle changes in the fluorescence lifetime distributions of the tryptophan probe at either position 240*c* or 145*r*. These observations cannot be ascribed to a major structure rearrangement, as observed with the 240's loop or the r1−c4 interface upon PALA binding (*3*, *68*), but merely reflect local changes in the side chain orientations of some neighboring residues. A cluster of amino acid interactions involving residues 146−149 of the regulatory chain and residues 242−245 of the catalytic chain was identified as one of the structural features involved in the transmission of the ATP regulatory signal (*19*, *26*). The involvement of the r1−c4 interface in ATP activation was further confirmed by the properties of chimeric ATCases (*40*, *41*). In the unliganded ATCase enzyme, the guanidinium group of Arg229*c*, a residue involved in aspartate binding, has been shown by X-ray crystallography to reorient toward the catalytic site upon ATP binding (*3*). This manifestation of the primary effect of ATP was assumed to be relayed by the 240's loop through the r1−c4 interface. The fluorescence data obtained with the Trp probes at positions 145*r* and 240*c* can readily be interpreted within this scheme, acting through a primary effect on the active site. X-ray solution scattering studies conducted in the presence of substoichiometric amounts of PALA showed that ATP does not shift the T to R equilibrium toward R (*18*, *43*), and equilibrium isotope studies demonstrated that ATP essentially acts by increasing the binding rate constant k_{on} of aspartate (*69*).

(b) CTP Inhibition. Contrary to ATP binding, the presence of the feedback inhibitor CTP does not modify the fluorescence properties of Trp at position 240*c*. On the other hand, the level of solvent exposure of the fluorescence probe at position 153*r* and to a minor degree at 145*r* is increased upon CTP binding. Thus, the environment of the C-terminal region of the regulatory chain has to be changed to some extent by the inhibitor nucleotide. However, the available crystal structures of the T-state, either unliganded (6AT1) or ligated to CTP (1RAI), do not show significant conformation changes in the C-terminal part of the regulatory chain, except if one admits that in the absence of any ligand the last three residues of the regulatory chain adopt a conformation close to that recently described for the R-state (1D09) (*62*). Only the binding of CTP would allow the C-terminal region to retract slightly from the hydrophobic interface as described in the high-resolution data of ATCase complexed to CTP (1RAI) (*70*). This movement could facilitate a minor closure of the allosteric−zinc interface, which is known to participate in the regulatory mechanism (*26*, *63*), and the stabilization of the T-state. The nature of the side chain of residue 153*r* does not interfere with CTP inhibition; however, deleting the last two C-terminal regulatory chain residues abolishes CTP inhibition and greatly reduces the level of ATP activation, an observation which is to be expected for an enzyme with a destabilized T-state (*26*).

In the work presented here, we demonstrate that the T to R transition can be monitored by the fluorescence properties of a Trp probe at position 145*r* close to the r1−c4 interface, thereby opening the way to investigation of the dynamics of this structure transition by spectroscopy. ATP activation induces local conformational changes at the r1−c4 interface which are further transmitted to the catalytic site without acting directly on the T to R transition. CTP inhibition involves, at least in part, direct effects on the T to R transition mediated by hinge bending motions of the allosteric and zinc domains of the regulatory chain.

ACKNOWLEDGMENT

We thank Moncef M. Ladjimi for the gift of the W209F/W284F mutant plasmid, Françoise Van Vliet for the generous gift of the W209F/W284F/F145*r*W and W209F/W284F/N153*r*W mutants, and Patrice Vachette for interesting discussions and valuable comments on the manuscript.

REFERENCES

1. Freire, E. (2000) *Proc. Natl. Acad. Sci. U.S.A. 97*, 11680−11682.
2. Hervé, G. (1989) in *Allosteric Enzymes* (Hervé, G., Ed.) pp 61−79, CRC Press, Boca Raton, FL.
3. Lipscomb, W. N. (1994) *Adv. Enzymol. 68*, 67−152.
4. Reichard, P., and Hanshoff, G. (1956) *Acta Chem. Scand. 10*, 548−566.
5. Gerhart, J. C., and Schachman, H. K. (1965) *Biochemistry 4*, 1054−1062.
6. Gerhart, J. C., and Pardee, A. B. (1962) *J. Biol. Chem. 237*, 891−896.
7. Bethell, M. R., Smith, K. E., White, J. S., and Jones, M. E. (1968) *Proc. Natl. Acad. Sci. U.S.A. 60*, 1442−1444.
8. Monod, J., Wyman, J., and Changeux, J. P. (1965) *J. Mol. Biol. 12*, 88−118.
9. Honzatko, R. B., Crawford, J. L., Monaco, H. L., Ladner, J. E., Ewards, B. F. P., Evans, D. R., Warren, S. G., Wiley, D. C., Ladner, R. C., and Lipscomb, W. N. (1982) *J. Mol. Biol. 160*, 219−263.
10. Ke, H., Honzatko, R. B., and Lipscomb, W. N. (1984) *Proc. Natl. Acad. Sci. U.S.A. 81*, 4037−4040.
11. Krause, K. L., Volz, K. W., and Lipscomb, W. N. (1987) *J. Mol. Biol. 193*, 527−553.
12. Svergun, D. I., Barberato, C., Koch, M. H., Fetler, L., and Vachette, P. (1997) *Proteins 27*, 110−117.
13. Wild, J. R., Loughrey-Chen, S. J., and Corder, T. S. (1989) *Proc. Natl. Acad. Sci. U.S.A. 86*, 46−50.
14. Howlett, G. J., Blackburn, M. N., Compton, J. G., and Schachman, H. K. (1977) *Biochemistry 16*, 5091−5099.
15. Schachman, H. K. (1988) *J. Biol. Chem. 263*, 18583−18586.
16. Thiry, L., and Hervé, G. (1978) *J. Mol. Biol. 125*, 515−534.
17. Tauc, P., Leconte, C., Kerbiriou, D., Thiry, L., and Hervé, G. (1982) *J. Mol. Biol. 155*, 155−168.
18. Hervé, G., Moody, M. F., Tauc, P., Vachette, P., and Jones, P. T. (1985) *J. Mol. Biol. 185*, 189−199.
19. Xi, X. G., Van Vliet, F., Ladjimi, M. M., De Wannemaeker, B., De Staerke, C., Glansdorff, N., Piérard, A., Cunin, R., and Hervé, G. (1991) *J. Mol. Biol. 220*, 789−799.
20. Stevens, R. C., and Lipscomb, W. N. (1992) *Proc. Natl. Acad. Sci. U.S.A. 89*, 5281−5285.
21. Lakowicz, J. R. (1999) *Principles of Fluorescence Spectroscopy*, Plenum Press, New York.
22. Fetler, L., Vachette, P., Hervé, G., and Ladjimi, M. M. (1995) *Biochemistry 34*, 15654−15660.
23. Eisenstein, E., Markby, D. W., and Schachman, H. K. (1989) *Proc. Natl. Acad. Sci. U.S.A. 86*, 3094−3098.

24. Newton, C. J., and Kantrowitz, E. R. (1990) *Proc. Natl. Acad. Sci. U.S.A. 87*, 2309−2313.
25. Xi, X. G., Van Vliet, F., Ladjimi, M. M., De Wannemaeker, B., De Staercke, C., Piérard, A., Glansdorff, N., Hervé, G., and Cunin, R. (1990) *J. Mol. Biol. 216*, 375−384.
26. De Staercke, C., Van Vliet, F., Xi, X. G., Rani, C. S., Ladjimi, M., Jacobs, A., Triniolles, F., Herve, G., and Cunin, R. (1995) *J. Mol. Biol. 246*, 132−143.
27. Ladjimi, M. M., and Kantrowitz, E. R. (1988) *Biochemistry 27*, 276−283.
28. De Staercke, C. (1994) Ph.D. Thesis, Vrije Universiteit Brussel, Brussels.
29. Perbal, B., and Hervé, G. (1972) *J. Mol. Biol. 70*, 511−529.
30. Fetler, L., Tauc, P., Hervé, G., Ladjimi, M. M., and Brochon, J.-C. (1992) *Biochemistry 31*, 12504−12513.
31. Collins, K. D., and Stark, G. R. (1971) *J. Biol. Chem. 246*, 6599−6605.
32. Jacobson, G. R., and Stark, G. R. (1973) *J. Biol. Chem. 248*, 8003−8014.
33. O'Connor, D. V., and Philipps, D. (1984) *Time Correlated Single Photon Counting*, Academic Press, New York.
34. Moya, I., Hodges, M., and Barbet, J.-C. (1986) *FEBS Lett. 198*, 256−262.
35. Brochon, J. C., Tauc, P., Mérola, F., and Schoot, B. (1992) *Biophys. J. 61*, A179.
36. Brochon, J.-C., Tauc, P., Mérola, F., and Schoot, B. M. (1993) *Anal. Chem. 65*, 1028−1034.
37. Brochon, J.-C. (1994) *Methods Enzymol. 240*, 262−311.
38. Livesey, A. K., and Brochon, J. C. (1987) *Biophys. J. 52*, 693−706.
39. Deprez, E., Tauc, P., Leh, H., Mouscadet, J. F., Auclair, C., and Brochon, J. C. (2000) *Biochemistry 39*, 9275−9284.
40. Cunin, R., Wales, M. E., Van Vliet, F., De Staercke, C., Scapozza, L., Rani, C. S., and Wild, J. R. (1996) *J. Mol. Biol. 262*, 258−269.
41. Cunin, R., Rani, C. S., Van Vliet, F., Wild, J. R., and Wales, M. (1999) *J. Mol. Biol. 294*, 1401−1411.
42. Teale, F. W. J., and Weber, G. (1957) *Biochem. J. 65*, 476−482.
43. Fetler, L., Tauc, P., Hervé, G., Moody, M. F., and Vachette, P. (1995) *J. Mol. Biol. 251*, 243−255.
44. Valeur, B., and Weber, G. (1977) *Photochem. Photobiol. 25*, 441−444.
45. Kirschner, M. W., and Schachman, H. K. (1973) *Biochemistry 12*, 2997−3004.
46. Johnson, R. S., and Schachman, H. K. (1980) *Proc. Natl. Acad. Sci. U.S.A. 77*, 1995−1999.
47. Hu, C. Y., Howlett, G. J., and Schachman, H. K. (1981) *J. Biol. Chem. 256*, 4998−5004.
48. Wacks, D. B., and Schachman, H. K. (1985) *J. Biol. Chem. 260*, 11651−11658.
49. Chen, Y., Liu, B., Yuy, H.-T., and Barkley, M. D. (1996) *J. Am. Chem. Soc. 118*, 9271−9278.
50. Chen, Y., and Barkley, M. D. (1998) *Biochemistry 37*, 9976−9982.
51. Beechem, J. M., and Brand, L. (1985) *Annu. Rev. Biochem. 54*, 43−71.
52. Szabo, A. G., and Rayner, D. M. (1980) *J. Am. Chem. Soc. 102*, 554−563.
53. Merola, F., Rigler, R., Holmgren, A., and Brochon, J. C. (1989) *Biochemistry 28*, 3383−3398.
54. Alcala, J. R., Gratton, E., and Prendergast, F. G. (1987) *Biophys. J. 51*, 587−596.
55. Ladjimi, M. M., Middleton, S. A., Kelleher, K. S., and Kantrowitz, E. R. (1988) *Biochemistry 27*, 268−276.
56. Roche, O., and Field, M. J. (1999) *Protein Eng. 12*, 285−295.
57. Beernink, P. T., Endrizzi, J. A., Alber, T., and Schachman, H. K. (1999) *Proc. Natl. Acad. Sci. U.S.A. 96*, 5388−5393.
58. Endrizzi, J. A., Beernink, P. T., Alber, T., and Schachman, H. K. (2000) *Proc. Natl. Acad. Sci. U.S.A. 97*, 5077−5082.
59. McMahon, L. P., Colucci, W. J., McLaughlin, M. L., and Barkley, M. D. (1992) *J. Am. Chem. Soc. 114*, 8442−8448.
60. Tsuruta, H., Vachette, P., Sano, T., Moody, M. F., Amemiya, Y., Wakabayashi, K., and Kihara, H. (1994) *Biochemistry 33*, 10007−10012.
61. Tsuruta, H., Sano, T., Vachette, P., Tauc, P., Moody, M. F., Wakabayashi, K., Amemiya, Y., Kimura, K., and Kihara, H. (1990) *FEBS Lett. 263*, 66−68.
62. Jin, L., Stec, B., Lipscomb, W. N., and Kantrowitz, E. R. (1999) *Proteins 37*, 729−742.
63. Ke, H., Lipscomb, W. N., Cho, Y., and Honzatko, R. B. (1988) *J. Mol. Biol. 204*, 725−748.
64. Ladjimi, M. M., Ghelis, C., Feller, A., Cunin, R., Glansdorff, N., Piérard, A., and Hervé, G. (1985) *J. Mol. Biol. 186*, 715−724.
65. Cherfils, J., Vachette, P., Tauc, P., and Janin, J. (1987) *EMBO J. 9*, 2843−2848.
66. Howlett, G. J., and Schachman, H. K. (1977) *Biochemistry 16*, 5077−5083.
67. Stevens, R. C., Gouaux, J. E., and Lipscomb, W. N. (1990) *Biochemistry 29*, 7691−7701.
68. Gouaux, J. E., and Lipscomb, W. N. (1990) *Biochemistry 29*, 389−402.
69. Hsuanyu, Y., and Wedler, F. C. (1988) *J. Biol. Chem. 263*, 4172−4181.
70. Kosman, R. P., Gouaux, J. E., and Lipscomb, W. N. (1993) *Proteins 15*, 147−176.
71. Berman, H. M., Westbrook, J., Feng, Z., Gilliland, G., Bhat, T. N., Weissig, H., Shindyalov, I. N., and Bourne, P. E. (2000) *Nucleic Acids Res. 28*, 235−242.

BI0029494